This is a postprint version of the following published document:

(Article begins on next page)

Multilayer Microstrip Closely-Spaced-Channel Wideband Diplexer With Highly-Selective Fourth-Order Filtering Responses

Li Yang, *Member*, *IEEE*, and Roberto Gómez-García, *Senior Member*, *IEEE*

Abstract—A type of multilayer microstrip diplexer with highly-selective wideband filtering channels is reported. Its closely-spaced fourth-order passbands are attributed to two circuit parts: (i) two third-order quasi-elliptic-type microstrip-to-microstrip wideband vertical transitions and (ii) a shunt two-stub dual-band bandpass filter (BPF) junction printed on the top layer. The two microstrip vertical transitions are developed by means of open-/short-circuit-ended microstrip lines and slotline stepped-impedance resonators (SIRs), respectively, and they correspond to the constituent lower and upper channels. The shunt dual-band BPF junction produces one additional transmission pole and one more pair of close-to-passband transmission zeros (TZs) for each channel to further increase their filtering selectivity. The RF theoretical foundations and design procedure of the engineered broadband diplexer are detailed. For practical-validation purposes, a proof-of-concept prototype of two-layer fourth-order microstrip wideband diplexer is simulated, manufactured, and tested. Its measured lower and upper channels has two closely-spaced sharp-rejection passbands with center frequencies of 1.496 GHz and 2.759 GHz and 3-dB fractional bandwidths of 62.83% and 24.83%, respectively, while featuring power-isolation levels above 27.39 dB from 0.5 to 4 GHz.

Index Terms—Bandpass filter (BPF), diplexer, microstrip filter, multilayer circuit, multiplexer, RF/microwave circuit, transmission zero (TZ), vertical transition, wideband circuit.
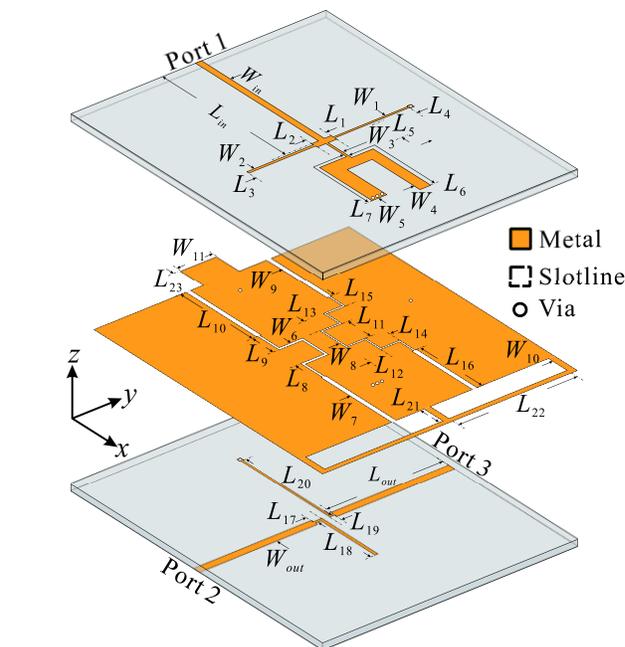

Fig. 1. 3-D layout of the proposed two-layer fourth-order microstrip diplexer made up of (i) two quasi-elliptic-type third-order wideband microstrip-to-microstrip vertical transitions using open-circuit-ended slotline SIRs and (ii) a shunt two-stub dual-band BPF junction.

I. INTRODUCTION

TO FACILITATE the development of emerging wideband/ultra-wideband communication systems, the exploration of novel high-performance microwave devices for their RF front-end chains is always requested [1]. As one of these key circuits, RF wideband diplexers connecting the transmitter and receiver modules are nowadays expected to feature not only low in-band insertion-loss and high power-isolation levels for their channels, but also sharp-rejection bandpass filter (BPF) actions into them.

Up to date, research efforts on RF wideband diplexers in planar and multilayer structures have been restricted to a very few solutions, such as those in [2]–[10]. For example, in [2]–[4], coupled open-loop and stub-loaded resonators were exploited

to develop microstrip wideband diplexers. By extending the upper-stopband bandwidth of the lower channel that is shaped by hybrid microstrip and slotline stepped-impedance resonators (SIRs), a wideband diplexer using broadside-coupled filters was designed in [5]. In [6], transversal signal-interference BPF sections were applied to design sharp-rejection microstrip wideband diplexers. In [7], by separately creating transmission zeros (TZs) at the upper and lower passband edges of the two relevant BPF channels with microstrip lines in bandstop mode, a high-selectivity wideband diplexer was realized. Besides, an alternative diplexer network made up of coplanar-waveguide wideband BPFs was discussed in [8]. Furthermore, based on multilayer superconducting quadrature hybrids in [9] and multilayer inductors in [10], respectively, wideband diplexers with compact circuit size were engineered. However, it is found that none of the aforementioned diplexer approaches features two closely-spaced channels with multiple close-to-passband TZs at both sides of the band edges. Although single-ended and balanced microstrip diplexers with pairs of close-to-passband TZs were proposed in [11] and [12], respectively, their usefulness is limited to narrow/moderate-bandwidth channels.
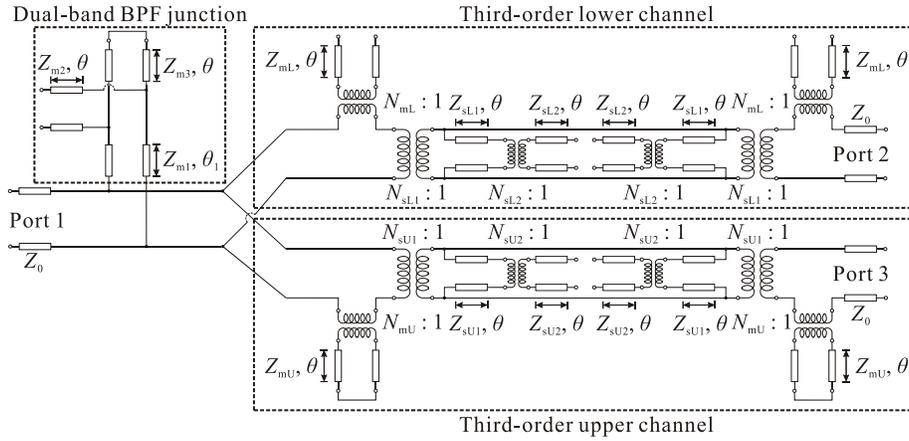
Fig. 2. TL equivalent circuit of the proposed two-layer fourth-order microstrip wideband diplexer shown in Fig. 1.

In this brief, a two-layer fourth-order microstrip diplexer with highly-selective wideband BPF channels is presented. It basically consists of a third-order wideband diplexer, in which the two building quasi-elliptic-type BPF channels are designed by means of microstrip-to-microstrip vertical transitions using open-circuit-ended slotline SIRs. Furthermore, by utilizing a dual-band BPF junction that is shunt connected at the input port of the third-order diplexer, one more transmission pole and two additional close-to-passband TZs are attained for each channel. In this manner, sharper-rejection capabilities when compared to its preliminary counterpart recently reported in [13] are attained. The analytical design methodology of the devised diplexer is detailed in Section II. In Section III, as practical validation, a two-layer microstrip diplexer prototype with highly-selective fourth-order wideband BPF channels is constructed and tested.

II. FOURTH-ORDER WIDEBAND DIPLEXER

The 3-D layout of the proposed two-layer fourth-order microstrip diplexer is depicted in Fig. 1. It consists of two main circuit parts: (i) a third-order wideband diplexer with two quasi-elliptic-type microstrip-to-microstrip vertical transitions using open-circuit-ended slotline SIRs and (ii) a shunt two-stub dual-band BPF junction loaded at the input port (Port 1). For the third-order wideband diplexer, the lower channel centered at f_L is realized by means of a microstrip vertical transition with open-circuit-ended microstrip lines being printed on the top and bottom layers and the open-circuit-ended slotline SIR etched at the common ground plane [14]. On the other hand, its upper channel operated at f_U is shaped by the other transition with short-circuit-ended microstrip lines and an open-circuit-ended slotline SIR. Besides, an open-circuit-ended microstrip line and a short-circuit-ended microstrip line are shunt connected by a non-resonant high-impedance microstrip segment, which acts as a dual-band BPF junction. Its main function is to create one more transmission pole and an extra pair of close-to-passband TZs for each channel of the constituent third-order diplexer to further enhance selectivity [15], [16]. To attain compact circuit size in the diplexer, the open-/short-circuit-ended microstrip resonators and slotline SIRs of the third-order diplexer, as well as the shunt open-/short-circuit-ended microstrip lines of the dual-band BPF junction, are realized by using folded structures. Moreover, the ground planes of two open-circuit-ended slotline

SIRs of the two channels are connected as a common ground plane by using a microstrip T-junction.

Based on the proposed diplexer in Fig. 1, its transmission-line (TL) equivalent circuit can be obtained as depicted in Fig. 2. As shown, the open-/short-circuit-ended microstrip resonators and the open-circuit-ended slotline SIRs of the third-order diplexer are represented by the in-series open-/short-circuit-ended TL stubs and the shunt TL segments cascaded by the open-circuit-ended TL stubs, respectively. Their impedance-line parameters are set as Z_{mL}, Z_{sL1}, and Z_{sL2} for the lower channel and as Z_{mU}, Z_{sU1}, and Z_{sU2} for the upper channel. Besides, the shunt open-/short-circuit-ended microstrip lines of the dual-band BPF junction are also replaced in the equivalent TL circuit by the relevant open-/short-circuit-ended TL stubs, but with different impedances Z_{m2} and Z_{m3}. Its non-resonant microstrip line is substituted by one TL segment with characteristic impedance Z_{m1} and electrical length θ_1 at $f_U/2$. Note that, except the non-resonant TL segment, all the other TL stubs and sections have an electrical length $\theta = 90°$, but at different design frequencies. Specifically, the design frequency for the third-order lower BPF channel and the short-circuit-ended stub of the dual-band BPF junction is selected as f_L. On the other hand, the design frequency of the TLs of the other channel and the open-circuit-ended stub of the dual-band BPF junction is chosen as $f_U/2$. Moreover, in order to properly model the impedance variations of the coupled microstrip lines and slotline SIRs of the third-order diplexer in the electromagnetic (EM) simulation, two sets of transformers are utilized with turns ratios of N_{mL}, N_{sL1}, and N_{sL2} for the lower channel and of N_{mU}, N_{sU1}, and N_{sU2} for the upper channel [17].

A. Third-Order Wideband Diplexer

In order to determine the RF operational foundations of the conceived overall wideband diplexer, its constituent third-order diplexer shaped by two quasi-elliptic-type wideband BPFs is theoretically analyzed first. With the *ABCD* submatrices of the two-port networks of the lower and upper channels in Fig. 2, their relevant characteristic functions F_L and F_U are derived as

$$F_L = j(\frac{z_{mL}'^2}{z_{sL}'}\cot^2\theta - z_{mL}'\cot\theta + \frac{1}{z_{sL}'}) \qquad (1)$$

$$F_U = j(\frac{z_{mU}'^2}{z_{sU}'}\tan^2\theta + z_{mU}'\tan\theta + \frac{1}{z_{sU}'}) \qquad (2)$$
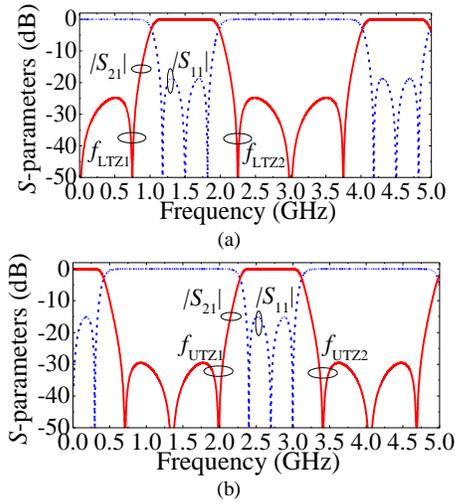
(a)

(b)

Fig. 3. Theoretical power transmission ($|S_{21}|$) and input-reflection ($|S_{11}|$) responses of the two-port third-order quasi-elliptic-type wideband BPFs associated to the lower and upper channels in Fig. 2 ($N_{mL} = N_{sL1} = N_{sL2} = N_{mU} = N_{sU1} = N_{sU2} = 1$). (a) Wideband BPF of the lower channel centered at $f_L = 1.5$ GHz ($z_{mL} = 2.031$ and $z_{sL1} = z_{sL2} = 1.6754$). (b) Wideband BPF of the upper channel centered at $f_U = 2.7$ GHz ($z_{mU} = 2.4485$, $z_{sU1} = 1.5166$, and $z_{sU2} = 1.7958$).

where

$$z'_{mL} = N_{mL}^2 \times z_{mL} \ \& \ z'_{mU} = N_{mU}^2 \times z_{mU} \quad (3)$$

$$z'_{sL} = N_{sL1}^2 \times \frac{z_{sL1}^2 \tan\theta - (N_{sL2}^2 \times z_{sL2})z_{sL1}\cot\theta}{z_{sL1} + N_{sL2}^2 \times z_{sL2}} \quad (4)$$

$$z'_{sU} = N_{sU1}^2 \times \frac{z_{sU1}^2 \tan\theta - (N_{sU2}^2 \times z_{sU2})z_{sU1}\cot\theta}{z_{sU1} + N_{sU2}^2 \times z_{sU2}}. \quad (5)$$

Here, z_{mL}, z_{sL1}, z_{sL2}, z_{mU}, z_{sU1}, and z_{sU2} are the normalized-impedance variables. By imposing that $F_L \rightarrow \infty$ and $F_U \rightarrow \infty$ with (1) and (2) as TZ-generation conditions, the TZ locations of the two-port third-order wideband lower and upper BPF channels are derived. Firstly, the intrinsic TZs of the lower BPF channel appear at $2nf_L$ with $n \in \mathbb{N}$, which are produced by the open-circuit-ended stubs. Due to the open-circuit-ended slotline SIR, two extra close-to-passband TZs appear at

$$f_{LTZ1} = 2f_L \frac{\tan^{-1}\sqrt{\dfrac{N_{sL2}^2 \times z_{sL2}}{z_{sL1}}}}{\pi} + 2nf_L \quad (6)$$

$$f_{LTZ2} = 2(n+1)f_L - 2f_L \frac{\tan^{-1}\sqrt{\dfrac{N_{sL2}^2 \times z_{sL2}}{z_{sL1}}}}{\pi}. \quad (7)$$

For the two-port upper BPF channel, its TZs created by the short-circuit-ended stubs are located at $(2n+1)f_U/2$. Similarly, two additional close-to-passband TZs are produced by its employed slotline SIR, whose spectral locations are

$$f_{UTZ1} = (n+1)f_U - f_U \frac{\tan^{-1}\sqrt{\dfrac{N_{sU2}^2 \times z_{sU2}}{z_{sU1}}}}{\pi} \quad (8)$$

$$f_{UTZ2} = (n+1)f_U + f_U \frac{\tan^{-1}\sqrt{\dfrac{N_{sU2}^2 \times z_{sU2}}{z_{sU1}}}}{\pi}. \quad (9)$$
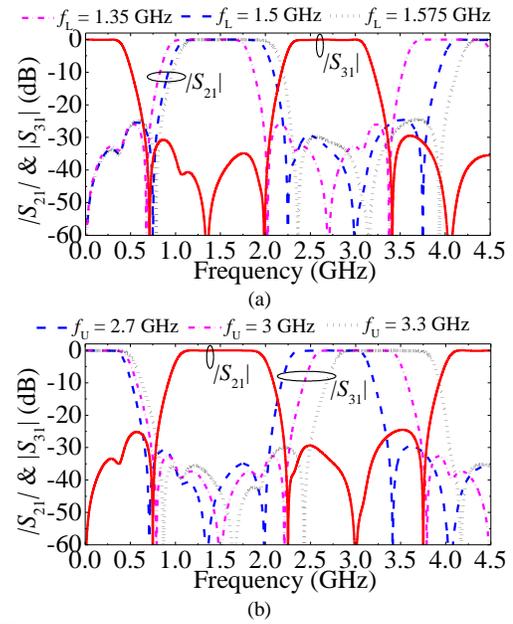

(a)

(b)

Fig. 4. Theoretical power transmission ($|S_{21}|$ and $|S_{31}|$) responses of the constituent third-order diplexer in Fig. 2 ($z_{mL} = 2.031$, $z_{sL1} = z_{sL2} = 1.6754$, $z_{mU} = 2.4485$, $z_{sU1} = 1.5166$, $z_{sU2} = 1.7958$, and $N_{mL} = N_{sL1} = N_{sL2} = N_{mU} = N_{sU1} = N_{sU2} = 1$). (a) Lower channel centered at different frequencies ($f_L = 1.35$, 1.5, and 1.575 GHz) and the upper channel being fixed ($f_U = 2.7$ GHz). (b) Upper channel centered at different frequencies ($f_U = 2.7$, 3, and 3.3 GHz) and the lower channel being fixed ($f_L = 1.5$ GHz).

From the above discussions, frequency responses of these two-port BPF channels are synthetically designed. In this example, the wideband BPF associated to the lower channel is expected to be centered at $f_L = 1.5$ GHz with relative bandwidth of $(f_{LTZ2} - f_{LTZ1})/f_L = 100\%$, passband ripple of 0.059 dB–or minimum in-band power-matching level of 18.723 dB–, and stopband attenuation levels above 24.788 dB. Besides, the wideband BPF acting as the upper channel is set to be centered at $f_U = 2.7$ GHz with fractional bandwidth of $(f_{UTZ2} - f_{UTZ1})/f_U = 52.67\%$, in-band power-matching levels above 15.084 dB, and out-of-band rejection levels higher than 29.59 dB. Hence, the impedance variables of the slotline SIRs are determined as $z_{Ls1} = z_{Ls2}$ and $z_{Us2} = 1.1841z_{Us1}$, respectively. To realize the specified responses for the BPFs of the two channels, their normalized-impedance values are selected as $z_{mL} = 2.031$ and $z_{sL1} = z_{sL2} = 1.6754$, and $z_{mU} = 2.4485$, $z_{sU1} = 1.5166$, and $z_{sU2} = 1.7958$. As shown in Fig. 3, the close-to-passband TZs for the lower and upper wideband BPFs appear at 0.75 GHz and 2.25 GHz and at 1.989 GHz and 3.411 GHz, respectively, in accordance with the theoretical predictions. The attainment of quasi-elliptic-type responses for both BPFs is also verified. Subsequently, the frequency responses of the whole third-order diplexer channels designed with these two wideband BPFs are illustrated in Fig. 4. Note that both the TZ positions and quasi-elliptic-type profiles are preserved for both closely-spaced channels with regard to the isolated BPFs. Specifically, Fig. 4(a) depicts the frequency responses of the lower channel for several center frequencies ($f_L = 1.35$, 1.5, and 1.575 GHz) and the upper channel being fixed ($f_U = 2.7$ GHz). As observed, the bandwidth of the lower channel is gradually enlarged as f_L increases from 1.35 to 1.575 GHz. A similar trend is observed in Fig. 4(b) when the center frequency of the upper channel is varied ($f_U = 2.7$, 3, and 3.3 GHz) and the lower
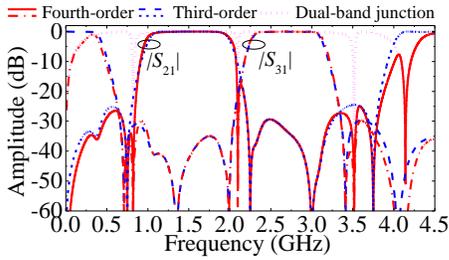
Fig. 5. Theoretical power transmission ($|S_{21}|$ and $|S_{31}|$) responses of the proposed overall highly-selective fourth-order wideband diplexer formed by the discussed third-order wideband diplexer in Fig. 4 and the shunt two-stub dual-band BPF junction ($Z_{m1} = 120\ \Omega$, $Z_{m2} = 35.5\ \Omega$, $Z_{m3} = 30.5\ \Omega$, and $\theta_1 = 58.11°$ at $f_U = 1.35$ GHz).
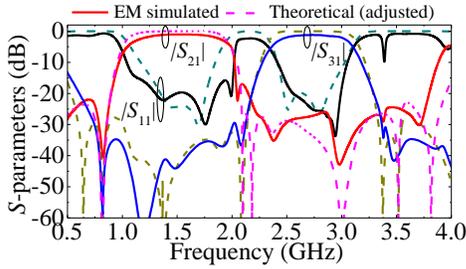

Fig. 6. EM-simulated and associated theoretical power transmission ($|S_{21}|$ and $|S_{31}|$) and input-reflection ($|S_{11}|$) responses of the proposed high-selective fourth-order microstrip wideband diplexer in Fig. 1 with the design dimensions of $L_{in} = 76.09$, $L_1 = L_2 = 2.09$, $L_3 = 30.673$, $L_4 = 34.875$, $L_5 = 13.5$, $L_6 = 37.64$, $L_7 = 35.24$, $L_8 = 9.2$, $L_9 = 12.4$, $L_{10} = 40$, $L_{11} = 9.76$, $L_{12} = L_{14} = 8.59$, $L_{13} = 5.12$, $L_{15} = 9.84$, $L_{16} = 37.04$, $L_{17} = 2.5$, $L_{18} = 29.57$, $L_{19} = 1.5$, $L_{20} = 34.875$, $L_{21} = 18$, $L_{22} = 45.5$, $L_{23} = 20$, $L_{out} = 45.3$, $W_{in} = W_{out} = 1.82$, $W_1 = 0.22$, $W_2 = 0.4$, $W_3 = 0.15$, $W_4 = 3$, $W_5 = 3.7$, $W_6 = W_7 = 0.4$, $W_8 = 0.12$, $W_9 = 0.4$, $W_{10} = 2$, and $W_{11} = 18$ (unit: mm).

one is kept static ($f_L = 1.5$ GHz). In this case, a larger bandwidth is attained for the upper channel as f_U goes from 2.7 to 3.3 GHz. Note that the passband of each channel must be allocated within the stopband region of the other one, and that a frequency-contiguous behavior by setting the proper frequency ratio of f_U/f_L for these two channels can be attained while reasonably avoiding passband distortion as a design limit.

B. Shunt Dual-Band BPF Junction

To further increase the order and the selectivity levels of the two channels of the above building third-order diplexer, a shunt dual-band BPF junction connected at the input port is added, as depicted in Fig. 2. Its function is to bring one more transmission pole and two extra close-to-passband TZs to each channel [15], so that the overall wideband diplexer exhibits two highly-selective fourth-order broadband BPF channels. To demonstrate the effectiveness of this dual-band BPF junction, the formula of its input impedance is determined as below

$$Z_{in} = \frac{j[Z_{m1}^2 Z_{m2} \tan(\frac{\theta_1 \pi f}{90° f_U}) + Z_{m1} Z_{m2} Z_{m3} \tan(\frac{\pi f}{2 f_L} - a)]}{Z_{m1} Z_{m2} - Z_{m1} Z_{m3} \tan(\frac{\pi f}{f_U}) \tan(\frac{\pi f}{2 f_L}) - b} \quad (10)$$

where

$$a = Z_{m1}^2 Z_{m3} \tan(\frac{\theta_1 \pi f}{90° f_U}) \tan(\frac{\pi f}{f_U}) \tan(\frac{\pi f}{2 f_L}) \quad (11)$$

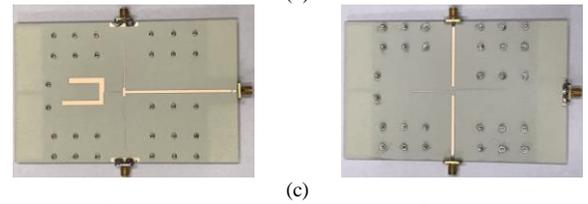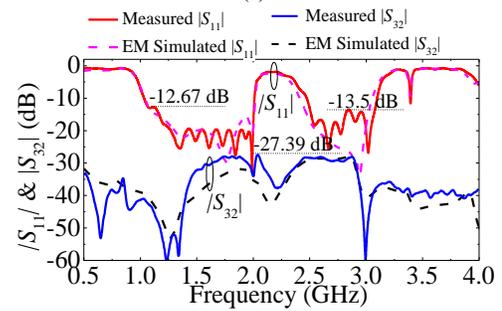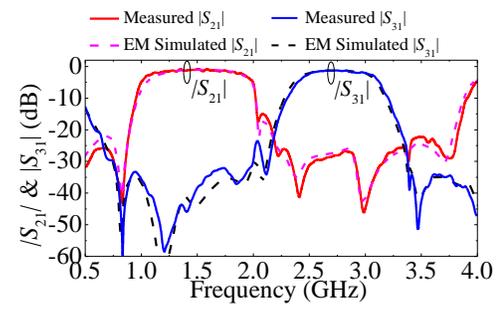$$b = Z_{m2} Z_{m3} \tan(\frac{\theta_1 \pi f}{90° f_U}) \tan(\frac{\pi f}{2 f_L}). \quad (12)$$

Fig. 7. Manufactured two-layer high-selective fourth-order microstrip wideband diplexer prototype with the layout shown in Fig. 1. (a) EM-simulated and measured power transmission ($|S_{21}|$ and $|S_{31}|$) responses. (b) EM-simulated and measured power input-reflection ($|S_{11}|$) and isolation ($|S_{32}|$) responses. (c) Photographs (top and bottom view) of the assembled diplexer prototype.

With the appropriately-chosen values $Z_{m1} = 120\ \Omega$, $Z_{m2} = 35.5\ \Omega$, $Z_{m3} = 30.5\ \Omega$, and $\theta_1 = 58.11°$ when $Z_{in} \to 0$, three TZs within the spectral interval from 0.5 to 4 GHz are introduced for each channel of the proposed fourth-order diplexer. As shown in Fig. 5, due to the dual-band BPF junction, the fourth-order lower BPF channel presents two more close-to-passband TZs at 0.822 GHz and 2.098 GHz, while the two extra TZs for the upper BPF channel are located at 2.098 GHz and 3.516 GHz. Compared with its constituent third-order wideband diplexer, the lower and upper channels of the overall fourth-order diplexer exhibit sharper roll-off stopband responses as merit.

III. IMPLEMENTATION AND DISCUSSION

In order to verify the experimental viability of the proposed fourth-order diplexer in Fig.1, a two-layer microstrip prototype is developed and tested. The engineered circuit is fabricated by a Rogers RO4003C substrate with relative dielectric constant $\varepsilon_r = 3.55$, dielectric thickness $h = 0.813$ mm, metal thickness $t = 35\mu m$, and dielectric loss tangent $\tan(\delta_D) = 0.0027$. To avoid undesired coupling between the ends of the open-circuit-ended slotline SIRs and the microstrip T-junction or the input-port microstrip segment on the common ground plane, their physical dimensions are properly adjusted during the EM simulation. The EM-simulated frequency responses of the fourth-order diplexer are plotted in Fig. 6. Here, the lower and upper channel

This article has been accepted for publication in IEEE Transactions on Circuits and Systems--II: Express Briefs. This is the author's version which has not been fully edited and content may change prior to final publication. Citation information: DOI 10.1109/TCSII.2022.3173910

> REPLACE THIS LINE WITH YOUR PAPER IDENTIFICATION NUMBER (DOUBLE-CLICK HERE TO EDIT) <   5

TABLE I
COMPARISON WITH OTHER PRIOR-ART MICROSTRIP WIDEBAND DIPLEXERS

Ref.	f_L/f_U (GHz)	Order	3-dB FBWs (%)	CTP TZs	PILs (dB)	Size ($\lambda_g \times \lambda_g$)
[2]	4.05/8.01	5/5	46.9/49.6	1/1	20	0.24×0.53
[3]	1.795/2.045	5/5	9.47/12.22	1/1	28	1.1×0.6
[6]	1.7/2.25	4/4	23.2/11.8	2/2	36	N/A
[7]	1.94/2.5	4/4	30/27	2/3	10.5	0.64×0.56
This Work	1.496/2.759	4/4	62.83/24.83	4/4	27.39	1.27×0.8

CTP: close-to-passband; PILs: power-isolation levels; λ_g: guided wavelength at the lower-channel center frequency of f_L.

are centered at 1.5 GHz and 2.73 GHz, respectively, being simulated with Z'_{mL} = 101.494 Ω, Z_{sL1} = Z_{sL2} = 87.76 Ω (lower channel), and Z'_{mU} = 122.37 Ω, Z_{sU1} = 74.31 Ω, Z_{sU2} = 86.65 Ω (upper channel). By adjusting the theoretical-design impedance values and imposing the re-calculated responses to closely meet to the EM-simulated ones [14], the turns ratios of the used transformers can be extracted as N_{mL} = 0.9997, N_{sL1} = 0.95, N_{sL2} = 1.15, and N_{mU} = 0.9998, N_{sU1} = 0.98, N_{sU2} = 0.85.

Fig. 7 depicts the measured results and the photographs of the built fourth-order wideband diplexer circuit. As shown, the measured lower and upper BPF channels feature the expected high-selectivity wideband BPF responses. Note also that a fairly-close agreement between EM-simulated and measured response is attained. The main performance metrics of two measured diplexer channels are as follows: lower BPF channel centered at f_L = 1.496 GHz with minimum in-band insertion-loss level of 0.79 dB and 3-dB passband from 1.026 to 1.966 GHz–i.e., fractional bandwidth of 62.83%; upper BPF channel centered at f_U = 2.759 GHz with minimum in-band insertion-loss level of 1.2 dB and 3-dB passband from 2.421 to 3.106 GHz–i.e., fractional bandwidth of 24.83%. Meanwhile, the measured maximum in-band group-delay variations of the two channels are 1.79 ns and 1.23 ns, respectively. In addition, the measured inter-channel power-isolation levels within the spectral interval from 0.5 to 4 GHz are higher than 27.39 dB. Furthermore, a comparison between the measured wideband diplexer in this work and other prior-art microstrip wideband diplexers is detailed in Table I. As can be seen, the developed diplexer prototype offers the best performance in terms of number of close-to-passband TZs for the two channels, which confer to them sharp-rejection filtering capabilities at both sides, along with remarkable power-isolation levels and order.

IV. CONCLUSION

A class of two-layer sharp-rejection fourth-order microstrip wideband closely-spaced-channel diplexer has been reported. Its core part is a third-order wideband diplexer designed with two quasi-elliptic microstrip-to-microstrip vertical transitions using open-circuit-ended slotline SIRs. In addition, to further increase the order and selectivity levels of its two BPF channels, a shunt two-stub dual-band BPF junction is added at its input. The RF operating principles of the proposed diplexer have been detailed. Finally, the devised broadband diplexer approach has been experimentally validated with a built two-layer fourth-order microstrip prototype with 1.496/2.759-GHz channels.

REFERENCES

[1] L. Zhu, S. Sun, and R. Li, *Microwave Bandpass Filters for Wideband Communications*. Hoboken, NJ, USA: Wiley, 2012.

[2] M.-H. Weng, C.-Y. Hung, and Y.-K. Su, "A hairpin line diplexer for direct sequence ultra-wideband wireless communications," *IEEE Microw. Wireless Compon. Lett.*, vol. 17, no. 7, pp. 519–521, Jul. 2007.

[3] Y. Wu, Y. Wang, and E. A. Ogbodo, "Microstrip wideband diplexer with narrow guard band based on all-resonator structures," in *Proc. 46th Eur. Microw. Conf.*, London, U.K., Oct. 2016, pp. 1163–1166.

[4] G.-Y. Wang, J.-J. Li, and C.-F. Chen, "Design of microstrip contiguous broadband diplexer based on dual-mode stub-loaded resonators," in *Proc. 2017 Asia-Pacific Microw. Conf.*, Kuala Lumpur, Malaysia , Nov. 2017, pp. 1007–1009.

[5] P. Deng, C. H. Chen, B. Huang, J. Jheng, H. Tung, and P. Chiu, "Design of wideband diplexer using broadside-coupled filters and stepped-impedance resonators," in *Proc. 2010 Asia-Pacific Microw. Conf.*, Yokohama, Japan, Dec. 2010, pp. 25–28.

[6] R. Gómez-García, J.-M. Muñoz-Ferreras, and M. Sánchez-Renedo, "Signal-interference stepped-impedance-line microstrip filters and application to duplexers," *IEEE Microw. Wireless Compon. Lett.*, vol. 2, no. 8, pp. 421–423, Aug. 2011.

[7] Y.-M. Xue, L. Yang, J.-X. Xu, X.-L. Zhao, and X. Y. Zhang, "Wideband diplexer with narrow channel spacing using hybrid bandpass-bandstop structures," *IEEE Access*, vol. 8, pp. 137783–137788, 2020.

[8] H. Jia and R. R. Mansour, "An efficient technique for tuning and design of filters and diplexers," *IEEE Trans. Microw. Theory Techn.*, vol. 68, no. 7, pp. 2610–2624, Jul. 2020.

[9] P. D. Laforge, R. R. Mansour, and M. Yu, "Diplexer design implementing highly miniaturized multilayer superconducting hybrids and filters," *IEEE Trans. Appl. Supercond.*, vol. 19, no. 2, pp. 47–54, Apr. 2009.

[10] S. Oshima, T. Kaho, Y. Yamaguchi, H. Shiba, and T. Nakagawa, "A wideband diplexer using multilayer inductors for compact wireless LTCC modules," in *Proc. 2014 IEEE Asia-Pacific Microw. Conf.*, Sendai, Japan, Nov. 2014, pp. 91–93.

[11] X. Guan, W. Liu, B. Ren, H. Liu, and P. Wen, "A novel design method for high isolated microstrip diplexers without extra matching circuit," *IEEE Access*, vol. 7, pp. 119681–119688, 2019.

[12] F. Wei, X. Y. Cheng, Y. X. Liu, and X. W. Shi, "Balanced-to-balanced diplexer and quadruplexer with high selectivity and wide CM suppression," *IEEE Trans. Circuits Syst. II*, *Exp. Briefs*, vol. 67, no. 11, pp. 2467–2471, Nov. 2020.

[13] L. Yang and R. Gómez-García, "Two-layered microstrip diplexer based on high-selectivity wideband bandpass filters," in *Proc. 2022 IEEE Radio Wireless Symp.*, Las Vegas, NV, USA, Jan. 16–19, 2022, pp. 146–149.

[14] L. Yang, L. Zhu, W.-W. Choi, K.-W. Tam, R. Zhang, and J. Wang, "Wideband microstrip-to-microstrip vertical transition with high filtering selectivity using open-circuited slotline SIR," *IEEE Microw. Wireless Compon. Lett.*, vol. 27, no. 4, pp. 329–331, Apr. 2017.

[15] C.-J. Chen, "A coupled-line coupling structure for the design of quasi-elliptic bandpass filters," *IEEE Trans. Microw. Theory Techn.*, vol. 66, no. 4, pp. 1921–1925, Apr. 2018.

[16] R. Gómez-García, L. Yang, J.-M. Muñoz-Ferreras, and D. Psychogiou, "Selectivity-enhancement technique for stepped-impedance-resonator dual-passband filters," *IEEE Microw. Wireless Compon. Lett.*, vol. 29, no. 7, pp. 453–455, Jul. 2019.

[17] L. Yang, L. Zhu, W.-W. Choi, and K.-W. Tam, "Analysis and design of wideband microstrip-to-microstrip equal ripple vertical transitions and their application to bandpass filters," *IEEE Trans. Microw. Theory Techn.*, vol. 65, no. 8, pp. 2866–2877, Aug. 2017